doi: 10.82124/CEAS-GNC-2026-054 CEAS-GNC-2026-054

Software and Hardware Validation of the Attitude Determination System of ST3LLARsat1 CubeSat Mission

Ghasem Sharifi Aerospace Engineering Department, Universidad Carlos III de Madrid (UC3M), Madrid, Spain

Diego Navarro-Tapia Aerospace Engineering Department, Universidad Carlos III de Madrid (UC3M), Madrid, Spain

Andrés Marcos Aerospace Engineering Department, Universidad Carlos III de Madrid (UC3M), Madrid, Spain

ABSTRACT

This paper presents a software and hardware validation of the attitude determination system for ST3LLARsat-1 BOIRA, the first student CubeSat developed at Universidad Carlos III de Madrid (UC3M). The study details the design of a dedicated photodiode configuration and a corresponding Sun-vector estimation algorithm. Moreover, an attitude determination framework based on the fusion of magnetometer, Sun vector, and gyroscope measurements was implemented using a quaternion-based extended Kalman filter (EKF), together with a method for monitoring filter convergence. Initial validation using model-in-the-loop simulation showed that, for the selected photodiode configuration, at least three photodiodes are illuminated for over 85% of the orbital time, keeping the Sun-vector estimation error below 5 deg. In addition, the EKF provided an RMS attitude estimation error of approximately 3 deg during eclipse, which represents the worst-case operating condition. The proposed convergence assessment method successfully identified unconverged filter behavior under intentionally disturbed conditions. Finally, the EKF was experimentally validated using an air-bearing free-rotation table to emulate a realistic operating scenario. By comparing the estimated attitude with the reference attitude obtained from an Attitude Heading and Reference System (AHRS), while using its internal sensor measurements as inputs to the developed EKF, the experimental results showed a maximum RMS attitude estimation error of 0.8 deg.

1 Introduction

ST3LLARsat1 “BOIRA” is the first student CubeSat developed at Universidad Carlos III de Madrid (UC3M). The primary objective of ST3LLARsat1 is to design, integrate, validate, launch, and operate a 2U CubeSat, mainly for educational purposes, with secondary objectives in technology demonstration and scientific exploration. One of the main technological goals of this mission is the implementation of an in-house Attitude Determination and Control System (ADCS) algorithm onboard. The mission involves two operational modes: detumbling, which aims to reduce the satellite’s angular velocity after deployment, and nadir pointing, which orients the satellite toward the Earth’s surface to achieve the desired attitude for payload operations.

Satellite attitude determination is a fundamental function of the ADCS subsystem, since accurate knowledge of the satellite orientation is required to achieve reliable pointing, stabilization, and closed-loop control performance. Among the available estimation approaches, Kalman-filter-based techniques have become one of the most widely used frameworks for attitude estimation because they provide a systematic means of combining dynamic models with noisy sensor measurements within an optimal or near-optimal stochastic estimation framework [1, 2]. In particular, the Extended Kalman Filter (EKF) has been extensively adopted for nonlinear attitude estimation problems, since satellite attitude kinematics are inherently nonlinear and are commonly represented using quaternions [3]. Quaternion-based EKF formulations are especially attractive because they avoid the singularities associated with Euler angles while preserving the computational efficiency required for embedded onboard implementation [3–5]. For this reason, Kalman-filter-based orientation estimation has been widely applied not only in spacecraft and aerial systems, but also in commercial inertial orientation units and attitude and heading reference systems (AHRS). Commercial products from manufacturers such as Xsens, MicroStrain, VectorNav, and Intersense have long relied on Kalman-filter-based sensor fusion architectures [6–9]. Motivated by these advantages, this work develops an EKF-based attitude determination algorithm for satellite applications by fusing gyroscope, magnetometer, and Sun-sensor measurements.

However, considering the history of satellite failures [10–12], the importance of subsystem level validation through hardware-in-the-loop (HIL) testing becomes evident. HIL testing replicates the space environment while incorporating actual ADCS components, thereby enabling a comprehensive evaluation of ADCS algorithms, sensors, and actuators under controlled and repeatable conditions. For tests requiring long-duration operation and flexibility in rotational degrees of freedom, air-bearing-based testbeds are among the most widely used platforms [13–16]. These systems support the test platform using pressurized air, providing nearly torque-free motion with minimal friction, and are therefore well suited for evaluating the dynamics and control performance of satellite attitude systems.

Previous work [17] presented the preliminary design of the ADCS, including the selection of sensors and actuators, as well as the placement of components within the satellite. Building upon that foundation, this work aims to develop and validate a satellite attitude determination system based on a quaternion-based EKF. In addition, an effective approach is proposed to assess the convergence status of the filter. The performance of the developed algorithm is first evaluated through software simulations, in which sensor characteristics, mission scenarios, environmental disturbances, and orbital conditions are modeled. Subsequently, the algorithm is validated experimentally through HIL testing using a rotational air-bearing platform under more realistic operating conditions and by comparison with a reference attitude sensor.

The article is organized as follows. Section 2 presents the ADCS architecture, components, and the photodiode configuration adopted for the satellite. Section 3 details the attitude determination algorithm and the corresponding mathematical formulation. Section 4 presents the simulation results, while the experimental results obtained from the HIL tests are described in Section 5. Finally, the conclusions and future work are presented in Section 6.

2 ADCS Design

2.1 ADCS Components

Considering the satellite stability and control requirements, which impose a pointing accuracy better than 10°, the attitude sensors were selected accordingly. To satisfy this requirement, the system incorporates a combination of coarse Sun sensors implemented with photodiodes, a magnetometer for measuring the magnetic field, and a gyroscope for angular rate sensing. In addition, a three-axis magnetic torquer is used as the actuator to generate the required control torque. To reduce the computational burden on the main onboard computer, the ADCS architecture includes a dedicated microcontroller for executing

the ADCS algorithms. The complete list of ADCS components is summarized in Table 1, together with their mass, power consumption, and duty cycle characteristics.

Table 1 ADCS mass and power budget [17].

Equipment	Model	Number	Mass (gr)	Power (mW)	Duty cycle(%)
Magnetometer	PNI RM3100-CB	1	0.25	2.2	20
Photodiode	OSRAM SFH 2401	13	0.043	0.065	100
Gyroscope	ADIS16500	1	1.75	200	100
GNSS	Orion B16-C1	1	1.7	215	100
Magnetorquer rods	CubeSpace CR0002	2	33	327	80
Magnetorquer coil	CubeSpace CubeCoil	1	46	600	80
Microcontroller	Microchip SAMV71Q21	1	1.365	297	100
Total			116.985	1969.24	

2.2 ADCS Architecture

The schematic of the ADCS architecture is presented in Fig. 1. The sensors are connected to the ADCS microcontroller and provide the input measurements, while the control commands generated by the ADCS are sent to the actuators (magnetic torquers) as outputs. In addition, a communication link exists between the satellite main onboard computer and the ADCS board to exchange information, including telemetry data to be transmitted to the ground station and high-level commands issued by the onboard computer. The algorithms implemented in the ADCS processor, which acts as the brain of the subsystem, include attitude determination, control, and orbit propagation.

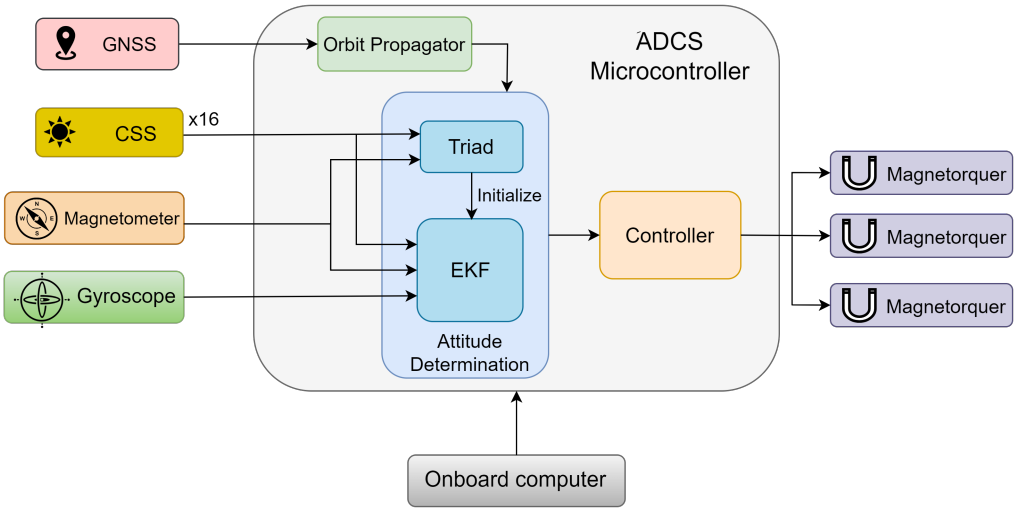

Fig. 1 Schematic diagram of the ADCS subsystem[17].

2.3 Photodiode Configuration

To estimate the Sun vector from photodiode measurements, at least three photodiodes must simultaneously observe the Sun under ideal conditions, i.e., in the absence of measurement noise. In practice, increasing the number of illuminated photodiodes improves the robustness and accuracy of the Sun vector estimation. Therefore, an analysis was carried out to determine the minimum number and arrangement of photodiodes required to ensure sufficient Sun visibility over the full range of satellite attitudes.

The output current of each photodiode reflects the amount of sunlight received on its active surface, which can be related to the Sun direction vector $\boldsymbol{S}_v$ with respect to the sensor normal vector $\boldsymbol{n}_s$. The current generated by each photodiode is modeled as

$$I = \begin{cases} I_{\max}(\boldsymbol{n}_s \cdot \boldsymbol{S}_v), & \text{if } (\boldsymbol{n}_s \cdot \boldsymbol{S}_v) > 0, \\ 0, & \text{if } (\boldsymbol{n}_s \cdot \boldsymbol{S}_v) \leq 0, \end{cases} \tag{1}$$

where $I_{\max}$ denotes the maximum current generated when the Sun is normal to the photodiode surface.

In this analysis, the Sun direction was varied parametrically over the full attitude domain, and the number of illuminated photodiodes was evaluated for each orientation. The results showed that a configuration consisting of 13 photodiodes, arranged as three on each lateral face and one on the top face, provides more than 85% Sun visibility with at least three illuminated sensors for almost all satellite orientations. The nadir face was excluded from the sensor placement due to the accommodation of the payload and communication antennas. The results of this analysis are presented in Fig. 2.

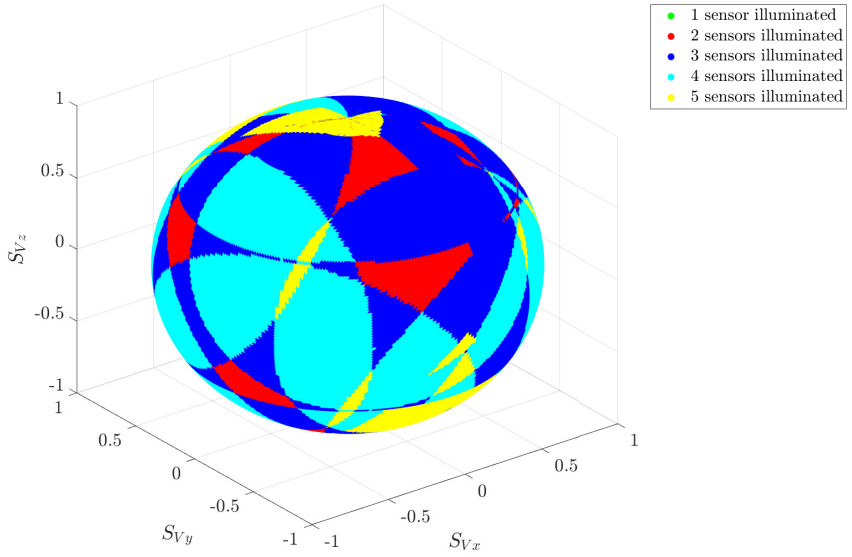

Fig. 2 Sun visibility analysis for the proposed photodiode configuration.

3 The Attitude Determination Methodology

3.1 Sun Vector Estimation

As described in Section 2, 13 photodiodes are used to estimate the Sun vector, $\hat{\boldsymbol{s}}$, for use in the attitude determination algorithm. Since the output of each photodiode is a current value that depends on the angle of the incident light relative to the sensor normal, an estimation algorithm is required to reconstruct the Sun vector from the set of photodiode measurements [18].

$$\hat{\boldsymbol{s}} = \frac{\sum_{i=1}^{N} \hat{C}_{k_i} V_i \hat{\mathbf{n}}_i \, [V_i > 0]}{\left\| \sum_{i=1}^{N} \hat{C}_{k_i} V_i \hat{\mathbf{n}}_i \, [V_i > 0] \right\|} \tag{2}$$

where N is the total number of photodiodes , V_i is the measured output of the i-th sensor, $\hat{C}_{k_i}$ is the estimated calibration scale factor of the i-th sensor, and $\hat{\mathbf{n}}_i$ is the unit normal vector of the i-th sensor

expressed in the body frame. The term $[V_i > 0]$ denotes the Iverson bracket, which is equal to 1 when the i-th sensor sees the Sun and 0 otherwise. Therefore, only sensors with positive illumination contribute to the estimate. The vector $\hat{\boldsymbol{s}}$ represents the estimated Sun-direction unit vector, obtained by normalizing the weighted sum of the sensor normal vectors.

3.2 Attitude Determination Equation

Attitude estimation was performed using a quaternion-based EKF, composed of prediction and correction steps. In the prediction stage, the quaternion is propagated using gyroscope measurements, while in the correction stage the estimate is updated using Sun sensor and magnetometer measurements. The corresponding nonlinear observation model and its Jacobian follow [2].

The prediction step is given by

$$\hat{\boldsymbol{q}}_t = f(\boldsymbol{q}_{t-1}, \boldsymbol{\omega}_{BI}), \tag{3}$$

$$\hat{P}_t = F_t P_{t-1} F_t^T + Q_t, \tag{4}$$

where $\hat{\boldsymbol{q}}_t$ is the predicted quaternion at time t, $\boldsymbol{q}_{t-1}$ is the quaternion estimate at the previous sampling instant, $\boldsymbol{\omega}_{BI}$ is the angular velocity of the body frame with respect to the inertial frame measured by the gyroscope, F_t is the state transition Jacobian, P_{t-1} is the estimation error covariance matrix at the previous step, and Q_t is the process noise covariance matrix.

The correction step is expressed as

$$\boldsymbol{q}_t = \hat{\boldsymbol{q}}_t + K_t \left(z_t - h(\hat{\boldsymbol{q}}_t) \right), \tag{5}$$

$$S_t = H_t \hat{P}_t H_t^T + R, \tag{6}$$

$$K_t = \hat{P}_t H_t^T S_t^{-1}, \tag{7}$$

$$P_t = (I_4 - K_t H_t) \hat{P}_t, \tag{8}$$

where $\boldsymbol{q}_t$ is the corrected quaternion estimate, $z_t = [\boldsymbol{S}_B^T \ \boldsymbol{B}_B^T]^T$ is the measurement vector composed of the Sun vector and magnetic field vector expressed in the body frame, $h(\hat{\boldsymbol{q}}_t)$ is the nonlinear observation model, H_t is its Jacobian matrix, K_t is the Kalman gain, R is the measurement noise covariance matrix, and P_t is the updated estimation error covariance matrix.

3.3 EKF Convergence Assessment

To evaluate the convergence and statistical consistency of the EKF, the normalized innovation squared (NIS) is evaluated using the innovation sequence generated during the correction step. The NIS at time t is computed as

$$\epsilon_t = \boldsymbol{\nu}_t^T S_t^{-1} \boldsymbol{\nu}_t, \tag{9}$$

$$\boldsymbol{\nu}_t = z_t - h(\hat{\boldsymbol{q}}_t), \tag{10}$$

where S_t is the innovation covariance matrix defined in Eq. (6). Under the assumption that the EKF is properly tuned and statistically consistent, the quantity ϵ_t follows a chi-square distribution with m degrees of freedom [19],

$$\epsilon_t \sim \chi_m^2, \tag{11}$$

where m is the dimension of the measurement vector z_t. Since z_t is composed of the Sun vector and geomagnetic field vector expressed in the body frame, the number of measurement components is $m = 6$.

Since the instantaneous NIS may fluctuate due to sensor noise, a more robust convergence indicator is obtained by considering its mean value over a window of N consecutive samples:

$$\bar{\epsilon}_t = \frac{1}{N} \sum_{i=t-N+1}^{t} \epsilon_i. \tag{12}$$

For a significance level α, the consistency interval of the mean NIS is defined as [19]

$$\frac{\chi^2_{\alpha/2,\,Nm}}{N} \leq \bar{\epsilon}_t \leq \frac{\chi^2_{1-\alpha/2,\,Nm}}{N}. \tag{13}$$

Based on this criterion, the EKF convergence flag is defined as

$$\text{flag}_t = \begin{cases} 1, & \text{if } \dfrac{\chi^2_{\alpha/2,\,Nm}}{N} \leq \bar{\epsilon}_t \leq \dfrac{\chi^2_{1-\alpha/2,\,Nm}}{N}, \\ 0, & \text{otherwise.} \end{cases} \tag{14}$$

Here, $\text{flag}_t = 1$ indicates that the innovation level is statistically consistent with the predicted innovation covariance over the selected window, and therefore the EKF is regarded as converged. Otherwise, $\text{flag}_t = 0$ indicates that the filter may still be in a transient regime or that the covariance matrices are not properly tuned.

4 Software Simulation

To assess the performance of the attitude determination algorithm, a model-in-the-loop (MIL) simulation was carried out. The parameters used in the software simulation to model the orbital environment, disturbance torques, and the satellite dynamics and kinematics are presented in Table 2.

Table 2 Mass Properties and Disturbance Parameters Used in MIL simulation.

Parameter	Symbol	Value	Parameter	Symbol	Value
MoI (x-axis)	I_x	$0.003\,\text{kg}\,\text{m}^2$	Residual dipole	m_r	$0.001\,\text{A}\,\text{m}^2$
MoI (y-axis)	I_y	$0.003\,\text{kg}\,\text{m}^2$	Solar Power	P_s	$1376\,\omega/\text{m}^2$
MoI (z-axis)	I_z	$0.001\,\text{kg}\,\text{m}^2$	Air density	ρ	$3.76 \times 10^{-12}\text{kg}/\text{m}^3$
Dimension	d	[0.1,0.1,0.2] cm	CoP and CoM offset	L_{mp}	1 cm
Mass	m	1.05 kg	Drag Coefficient	C_d	2
Altitude	Alt	500 km	Inclination	inc	97.12°

† MoI, COP and CoM denotes Moment of Inertia, Center of Pressure and Center of Mass respectively.

† ρ denotes the density under high solar activity.

The simulation results for Sun-vector estimation during the pointing phase using photodiodes are presented in Fig. 3. As shown in the top panel, the estimation error remains below approximately 5° during illuminated intervals. By comparing the top and middle panels, it can be observed that the estimation accuracy is directly related to the number of illuminated photodiodes, N_{illum}, with lower estimation error achieved when a larger number of photodiodes are illuminated simultaneously. Furthermore, the bottom panel shows the distribution of N_{illum}, indicating that in more than 85% of the illuminated cases, at least three photodiodes are active, which is the minimum number required for Sun-vector estimation.

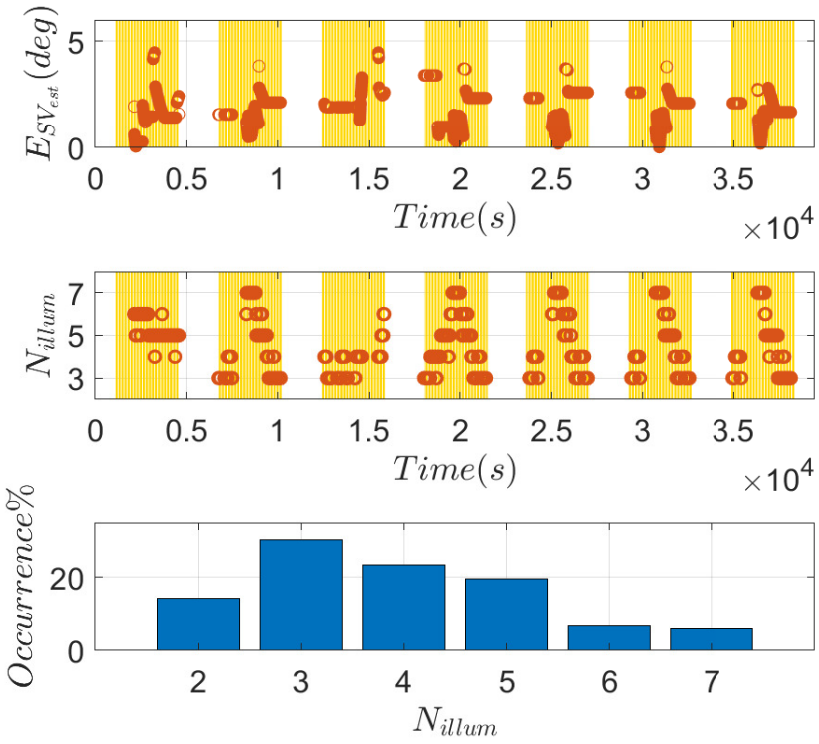

Fig. 3 Sun-vector estimation error (top), number of illuminated photodiodes at each sample time (middle), and occurrence of the number of illuminated photodiodes (bottom).

The attitude estimation error (E_{EKF}) obtained using the EKF in the pointing phase is presented in Fig. 4. The results show that the developed EKF is able to estimate the attitude accurately by fusing the available sensor measurements, achieving an RMS estimation error of approximately 3°. To further evaluate the EKF convergence status using the proposed normalized innovation squared (NIS)-based approach, an artificial magnetic disturbance was intentionally applied at t = 10,000 s for a duration of 10 s. As shown in the figure, the estimation error is relatively high during the initial stage, from t = 0 to approximately t = 100 s, due to filter initialization. After convergence, the estimation error decreases and remains below approximately 3°. When the magnetic disturbance is injected, the EKF estimation error temporarily increases, indicating a degradation in estimation performance.

For comparison, the convergence assessment was also performed using a covariance-based criterion derived from the rate of change of the diagonal elements of the covariance matrix P, where the filter is considered converged when this rate falls below a predefined threshold. The comparison shown in the bottom panel indicates that both the NIS-based and covariance-based criteria are sensitive to the initial convergence phase. However, only the NIS-based criterion is able to detect the temporary loss of consistency caused by the applied magnetic disturbance, whereas the covariance-based criterion remains almost unchanged. This demonstrates that the proposed NIS-based method provides a more sensitive and reliable indicator of EKF convergence and consistency, making it more suitable for determining whether the EKF estimates are reliable enough to be used in the control loop.

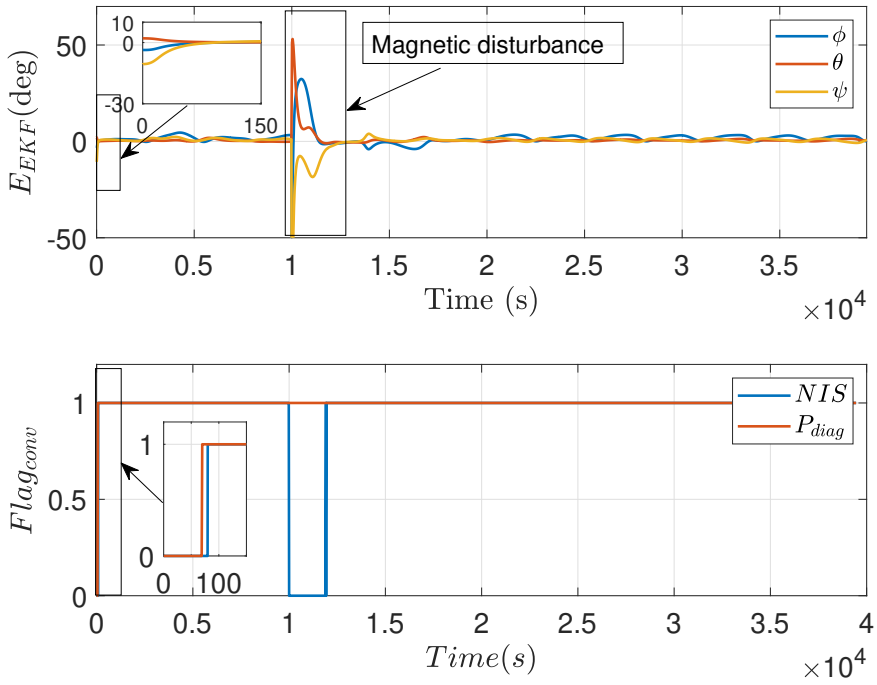

Fig. 4 EKF attitude estimation error for the three Euler angles (top) and convergence assessment flags obtained from the proposed NIS-based criterion and the covariance-diagonal-based criterion (bottom).

5 Experimental Testing

5.1 Experimental Setup

The experimental nanosatellite attitude control simulator (See Fig. 5) is used for the validation of the attitude determination and control subsystems, as well as for the verification of sensor and actuator outputs. The setup is particularly useful for attitude testing, allowing the evaluation of different sensor configurations. The main components of the setup include a rotational air bearing, an attitude and heading reference system (AHRS) serving as an attitude reference, an electronics subsystem comprising a power supply, and a wireless module for transmitting data to the ground computer. The setup provides three axes of rotation, with free rotation about the z-axis and a limitation of 20° about the x- and y-axes. The system is capable of testing CubeSats of up to 12U in size. The setup used for attitude testing is presented in Fig. 5.

5.2 HIL Validation Test of Attitude Determination

A HIL test was designed to assess attitude determination performance under a realistic scenario. For this purpose, an AHRS sensor integrating a magnetometer, accelerometer, and gyroscope, together with an internal EKF, was employed. The raw measurements from the internal sensors were fed into the developed algorithm, and the attitude estimated by the proposed EKF, $Euler_{est}$, was compared with the attitude output provided by the AHRS, $Euler_{AHRS}$. In this test, the accelerometer was used as a substitute for the Sun sensor. However, since the main objective was the validation of the estimation algorithm, the change in sensor type does not affect the purpose of the test. The test scenario is presented in Fig. 6.

The experimental results of the attitude determination test are presented in Fig. 7. The test was conducted under random initial conditions for both the angular velocity and the attitude of the setup. During the experiment, the setup was rotated about the z-axis, which allowed full rotation, while oscillatory

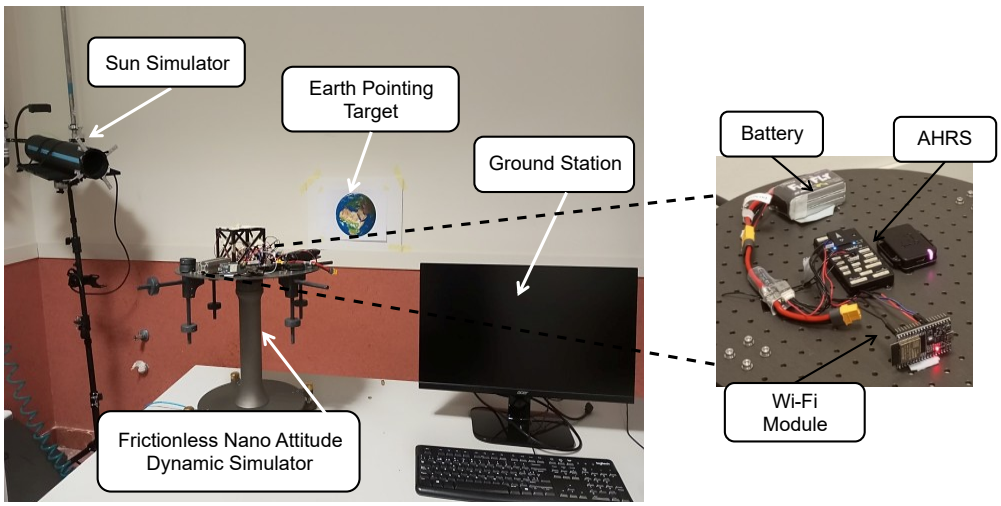

Fig. 5 Nano satellite attitude control simulator

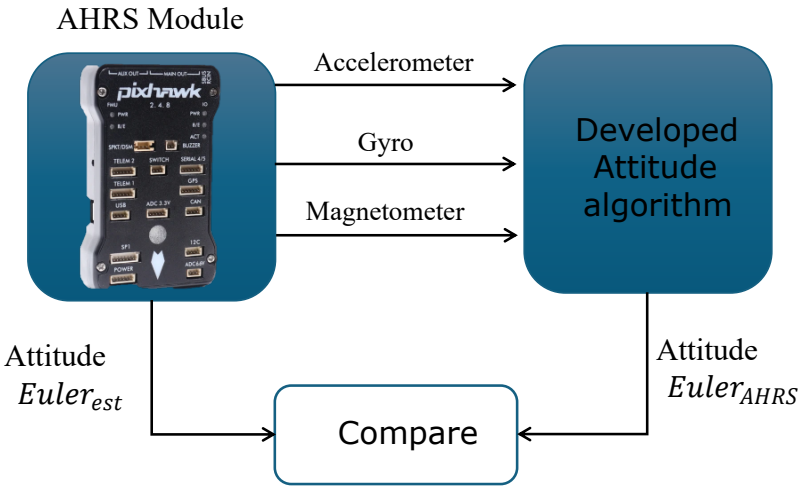

Fig. 6 Test scenario of the attitude determination validation.

motion was applied about the other two axes within a maximum range of ±10°, corresponding to the mechanical limitation of the test platform. As shown in the Fig. 7, the attitude estimated by the developed EKF closely tracks the AHRS output along all three axes. The estimation error is also presented, showing an RMS error of approximately 3° for the yaw axis and about 0.4° and 0.8° for the pitch and roll axes, respectively. A spike appears in the yaw error due to the angle wrapping that occurs when the rotation crosses from 180° to −180°. Overall, these results demonstrate that the developed algorithm provides sufficient accuracy for satellite attitude determination applications.

6 Conclusion

A software and hardware validation procedure for the attitude determination subsystem was carried out, including component selection, algorithm development, software simulation, and HIL testing. A quaternion-based EKF was developed to fuse magnetometer, Sun sensor, and gyroscope measurements. Simulation results showed that, under eclipse conditions representing the worst-case scenario, the proposed method achieved an RMS attitude estimation error of 3°. In addition, an approach was proposed to assess the convergence status of the EKF. By intentionally disturbing the system, the performance of the method was evaluated in detecting periods of non-convergence. To further strengthen the validation, an HIL test was performed using an air-bearing platform that enables three-axis rotational motion. In this setup, an AHRS unit was used as the attitude reference, and the results showed an RMS error of 0.8°.

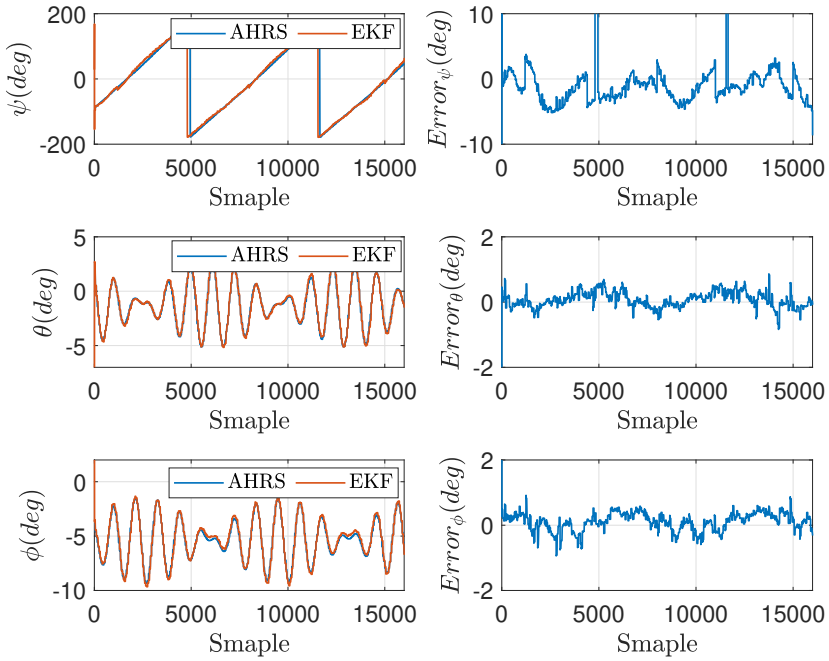

Fig. 7 Experimental validation results of the developed attitude determination algorithm.

To complete the validation process, the real satellite sensors are currently being characterized in order to evaluate the performance of the entire subsystem using the actual sensors together with the developed EKF algorithm. In addition, an experimental setup including a Sun simulator, an albedo simulator, and photodiodes mounted on the satellite structure is under development to experimentally validate the Sun vector estimation approach. These results will be presented in future work.

References

[1] R. E. Kalman. A new approach to linear filtering and prediction problems. *Journal of Basic Engineering*, 82:35–45, 1960.

[2] Angelo Maria Sabatini. Kalman-filter-based orientation determination using inertial/magnetic sensors: Observability analysis and performance evaluation. *Sensors*, 11(10):9182–9206, 2011. ISSN: 1424-8220. doi: 10.3390/s111009182.

[3] Angelo Maria Sabatini. Quaternion-based extended kalman filter for determining orientation by inertial and magnetic sensing. *IEEE Transactions on Biomedical Engineering*, 53(7):1346–1356, 2006. doi: 10.1109/TBME.2006.875664.

[4] João Luís Marins, Xiaoping Yun, Eric R. Bachmann, R. B. McGhee, and Michael J. Zyda. An extended kalman filter for quaternion-based orientation estimation using MARG sensors. In *Proceedings of the 2001 IEEE/RSJ International Conference on Intelligent Robots and Systems*, pages 2003–2011, 2001. doi: 10.1109/IROS.2001.976367.

[5] Itzhack Y. Bar-Itzhack, Julie Deutschmann, and F. Landis Markley. Quaternion normalization in additive EKF for spacecraft attitude determination. In *AIAA Guidance, Navigation, and Control Conference*, 1991. doi: 10.2514/6.1991-2706.

[6] Xsens Technologies B.V. *MTi and MTx User Manual and Technical Documentation*. Xsens Technologies B.V., Pantheon 6a, 7521 PR Enschede, The Netherlands, May 2009.

[7] MicroStrain Inc. *3DM-GX3-25 Miniature Attitude Heading Reference Sensor*. 459 Hurricane Lane, Suite 102, Williston, VT 05495, USA, 1.04 edition, 2009.

[8] VectorNav Technologies, LLC. *VN-100 User Manual*. College Station, TX 77840, USA, preliminary edition, 2009.

[9] InterSense, Inc. *InertiaCube2+ Manual*. 36 Crosby Drive, Suite 150, Bedford, MA 01730, USA, 1.0 edition, 2008.

[10] David Y. Kusnierkiewicz. An overview of the timed spacecraft. *Johns Hopkins APL Technical Digest*, 24(2):150–155, 2003.

[11] Brent P. Robertson, Phil Sabelhaus, Todd Mendenhall, and Lorraine M. Fesq. The recovery of toms-ep. 1998. `https://api.semanticscholar.org/CorpusID:106459801`.

[12] Mak Tafazoli. A study of on-orbit spacecraft failures. *Acta Astronautica*, 64(2):195–205, 2009. ISSN: 0094-5765. doi: https://doi.org/10.1016/j.actaastro.2008.07.019.

[13] Jana L. Schwartz, Mason A. Peck, and Christopher D. Hall. Historical review of air-bearing spacecraft simulators. *Journal of Guidance, Control, and Dynamics*, 26(4):513–522, 2003. doi: 10.2514/2.5085.

[14] Weiliang Zhu, Zhaojun Pang, and Zheng H. Zhu. Planar air-bearing microgravity testing for maneuverable space net deployment and retrieval with distributed cooperative control. *Acta Astronautica*, 236:1096–1100, 2025. ISSN: 0094-5765. doi: https://doi.org/10.1016/j.actaastro.2025.07.053.

[15] Tomasz Rybus, Hendrik Kolvenbach, and Xiu Tian Yan. Air-bearing microgravity simulators for space robotics. In Xiu Tian Yan and Gianfranco Visentin, editors, *Space Robotics: The State of the Art and Future Trends*, pages 157–190. Springer, Cham, Switzerland, 2024. doi: 10.1007/978-3-031-39214-6_8.

[16] Ghasem Sharifi, Sergio Garcia, and Gonzalo Sanchez-Arriaga. Validation of the attitude determination and control system of a deorbit device equipped with an electrodynamic tether using hardware in the loop testing. In *AIAA SCITECH 2026 Forum*, 2026. doi: 10.2514/6.2026-0213, `https://arc.aiaa.org/doi/abs/10.2514/6.2026-0213`.

[17] Ghasem Sharifi, Andrés Rabuñal-Gayo, Diego Navarro-Tapia, and Andrés Marcos. Development of an attitude determination and control strategy for the st3llarsat1 cubesat mission. In *Proc. SPIE 13546, Small Satellites Systems and Services Symposium (4S 2024)*, volume 13546, page 1354629. SPIE, Mar. 2025. doi: 10.1117/12.3061928, https://doi.org/10.1117/12.3061928.

[18] Stephen A. O'Keefe and Hanspeter Schaub. Sun-direction estimation using a partially underdetermined set of coarse sun sensors. *The Journal of the Astronautical Sciences*, 61(1):85–106, 2014. doi: 10.1007/s40295-015-0058-9.

[19] Yaakov Bar-Shalom, X. Rong Li, and Thiagalingam Kirubarajan. *Estimation with Applications to Tracking and Navigation: Theory, Algorithms, and Software*. John Wiley & Sons, New York, 2001. ISBN: 978-0-471-41655-5. doi: 10.1002/0471221279.